International Journal of Theoretical and Applied Research (IJTAR)
ISSN: 2812-5878

Homepage: https://ijtar.journals.ekb.eg

Original article

Effect of copper doping on the characterization, bioactivity, antibacterial, and cytotoxicity of akermanite-based glass ceramic

Basma Yousef El adawy [1*], Aida A. Salama [1], Heba S. Zayed [1], Mostafa Mabrouk [2], Esmat M.A. Hamzawy [3]

[1] *Faculty of Science, Al-Azhar University (Girls), Nasr City, Cairo, Egypt.*
[2] *Refractories, Ceramics and Building Materials Dept., National Research Centre, Dokki, Giza, Egypt.*
[3] *Glass Research Dept., National Research Centre, Dokki, Giza, Egypt.*

ARTICLE INFO

Received 18/02/2023
Revised 15/03/2023
Accepted 19/03/2023

Keywords

Akermanite
Cu_2O
Bioactivity
Antibacterial
Cytotoxicitys

ABSTRACT

Low-cost bioactive glass-ceramic, akermanite (Ca2MgSi2O7) with and without Cu2O was synthesized. Limestone, Silica sand, and Magnesium carbonate served as the parent materials. The prepared materials were investigated using various techniques (DTA, FTIR, XRD, SEM). Glass-ceramic samples were examined for bioactivity, degradation, and ion release in simulated body fluids (SBF). Additionally, the antibacterial impact was examined using *Escherichia coli*, *Staphylococcus aureus*, *Pseudomonas aeruginosa*, and *Klebsiella pneumonia*. Moreover, the cytotoxicity of Wi-38 cells lines, which are typical fibroblasts, was examined. According to DTA, the presence of Cu2O did not significantly raise the temperature at which glass crystallizes. The crystallization of the glasses into cuspidine, akermanite, and diopside was strong at 1000 ˚C. In a glassy matrix, nanosized clusters and submicron crystals can be seen in the microstructure. After immersion in SBF, all samples included nano and submicron hydroxyapatite particles. Bioactivity showed that all samples could form a hydroxyapatite layer after 2 or 4 weeks in SBF. The antibacterial results showed that all of the samples were antibacterial against the germs that were tested. Performing an MTT assay on samples to determine the cytotoxicity, all of the samples showed excellent cytocompatibility and cell proliferation and could be used safely in biomedical applications.

Graphical abstract

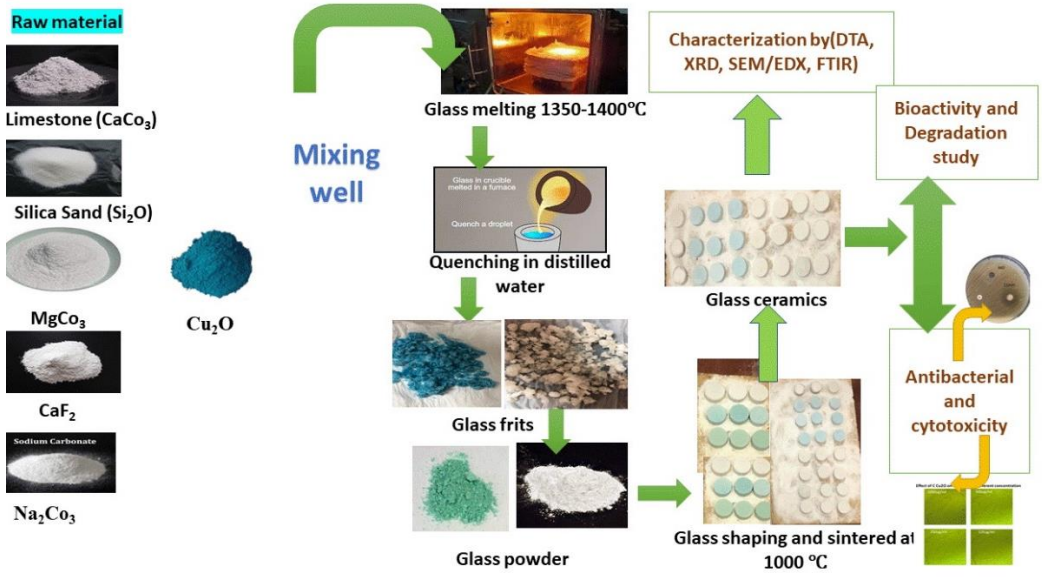

∗ *Corresponding author*
E-mail address:basmajoe2012@yahoo.com

DOI: 10.21608/IJTAR.2023.193677.1019

1. Introduction

Biomaterials are materials that have been produced and designed to work with biological systems. They are bioactive substances that quickly integrate into human tissue. They have good biodegradability. They are frequently employed in manufacturing processes for human body parts, medications, and tissue engineering. Many factors can cause critical bone problems, including necrosis, osteoporosis, trauma, tumor excision, and chronic inflammatory inflammation [1]. These defects do not repair themselves so, to create bioactive materials that can make contact with both hard and soft tissues, grow bone, and repair faults, many tool methods have been used [2]. The 45S5 bioactive glass was first made by L. L. Hench using the melt quenching technique at high temperatures (1200–1500 °C) [3]. To be successful implant materials, bioactive materials must have strong biocompatibility, postproductions, good degradation rate [4,5] and high mechanical strength [6,7]. Due to their capacity to generate hydroxyapatite (HA) layers in the (SBF), bioactive materials have been studied for applications in bone regeneration. Simulated body fluids have an ionic concentration that is similar to that of human blood plasma [8,9]. $Ca_{10}(PO_4)_6(OH)_2$ layers, often known as HA, is the major component of the human skeleton. In the last ten years, silicate glass-ceramics have been produced, including wollastonite ($CaSiO_3$), akermanite ($Ca_2MgSi_2O_7$), diopside ($CaMgSi_2O_6$), merwinite ($Ca_3MgSi_2O_8$) and bredigite ($Ca_7MgSi_4O_{16}$). It has been demonstrated that glass ceramics comprising CaO and SiO_2 can generate apatite that mimics bone and have excellent bioactivity for bone-to-implant materials [10].

The ability of materials to generate an interface layer of hydroxyapatite with living bone tissue and the release of soluble ions by these substances after their resorption is what gives them their bioactivity [11,12].

Additionally, due to the restricted mechanical qualities of current bioactive ceramics for bone tissue applications, researchers have concentrated on the development of unique bioactive replacement materials [11,13]. The production of bones depends on substances like silicon (Si), calcium (Ca), and magnesium (Mg), all of which are crucial to human health. The body of a typical adult weighing 70 kg has an estimated 1 mole of magnesium, making it the fourth most abundant cation in the human body. This is almost completely deposited in bone tissue. Although Ca is the main element present in bone tissues, human teeth, and amino acids, Mg and Si are necessary for the synthesis and growth of bone tissue for the skeleton, osteogenesis, and the creation of a new skeleton [14,15]. As a bioceramic that includes Ca, Mg, and Si, a stimulating effect of akermanite allows the inorganic ions it contains to be released into the tissue and promotes cell attachment to the bone and growth there [12,16]. Si and Mg ions' stimulating effects have a greater impact on the development of these cells than Ca ions do, in addition to the fact that Ca, Mg, and Si, ions could promote cell proliferation. Wu and Chang [17] noted that the ionic results derived by the dissolution of AK have a positive effect can create bone-like apatite in simulated body fluid.

Additionally, various experiments have been done to use higher ion concentrations than SBF to speed up the production of the apatite layer [18,19,20]. Due to its bioactive qualities in both vivo and vitro, AK is also a promising innovative bioceramic for biomedical applications [21]. Additionally, AK ceramics have a superior degradation rate [22], adjustable mechanical characteristics [23], and are biodegradable materials without cytotoxicity. The AK material has a variety of chemical compositions, which influences bio ceramics' features including biocompatibility and rapid degradation, and can be designed to satisfy the requirements of the chosen application area [23].

Another factor that is essential for the determination of the success of implants for medical applications is good antibacterial action. After being implanted in the body, microorganisms have the potential to cause pneumonia, skin infections, and wound infections. Antimicrobial agents must therefore be added to the bioactive substance. Numerous antibacterial substances, such as silver, zinc, copper, cerium, selenium, and, europium, have been researched in the previous literature [24,25,26]. Copper had many vital properties such as: (i) It plays a significant part in the osteoblastic cells' ability to grow [27]. (ii) It is less cytotoxic and works well as an antibiotic [28]. (iii) Also, Cu is a necessary ion for human health, and it has been shown to control angiogenesis [29]. (iv) Copper ions are well known for promoting embryonic osteogenic differentiation, angiogenesis, and cell growth [18](v) Copper is crucial for the growth and repair of bones [30]. Akermanite with and without copper was synthesized by the melt quenching method and the prepared samples were investigated for their characterization, SBF bioactivity, antimicrobial effect against gram-negative and gram-positive bacteria, and their cytotoxicity was evaluated.

2. Materials and Methods

2.1. Synthesis of (akermanite) glass ceramics with and without copper

Glass-ceramics are glass that has crystallized as a result of the thermal processing of its parent glass. Melt quenching is one of the typical processes used to create bioactive glasses [31,32]. According to earlier research, the akermanite and copper-doped akermanite powders were created in this work using the melt-quenching process. Akermanite was intended to form in the parent glass batch, but 5% Na_2O was added to lower the melting point. The initial materials were limestone, which has the following chemical composition in weight percent: CaO: 55.70, SiO_2: 0.15, Al_2O_3: 0.22, Fe_2O_3: 0.02. TiO2: 0.01, MgO: 0.02, Na_2O: 0.01, K_2O: 0.16 and loss ignition 44.02) silica sand SiO_2 (99.4 SiO_2, 0.04 CaO, 0.01 K_2O, 0.12 Fe_2O_3, 0.03 SO_3), $MgCO_3$ (Fluka Chemika, 98%-Switzerland), CaF2 (Laboratory Supplies Poole, BHI15ITD, Germany) and Na_2CO_3 (Fluka Analytical, Sigma-Aldrich, Germany). Over each 100 g of glass oxide that was used as the

base composition, copper oxide (Cu_2O) was added in two ratios (0.25% and 0.5%). The chemical composition of glass samples is displayed in Table 1 as a percentage of oxide weight. Each batch was blended for five hours in an agate grinding machine.

Homogeneous samples were melted in a platinum crucible for two hours at a temperature between 1350 and 1400 ºC. The bubble-free melted glass was poured into regular distilled water with a small amount of ethyl alcohol and quenched. Glass in the form of fine powder was produced by drying the glass frits and then powdering them in a grinding machine. Using a stainless-steel mold and uniaxial pressure of 20 KN for 60 s to obtain crack-free bodies, a polyvinyl alcohol powder (PVA 7%) was added as a binder, and the later glass powder was formed into discs (1 cm in diameter). The shaped discs were sintered in a single stage for two hours at 1000 ºC with a 10 ºC /min heating rate.

Table 1. Ionization energy of elements by Elsheekh Theory comparing with experimental data of (NIST).

Sample NO.	Chemical Composition Wt %				Additions over 100g glass oxide	
	CaO	MgO	SiO_2	CaF_2	Na_2O	Cu_2O
Ak0	19.04	13.67	40.94	26.50	4.28	-----
AK0.25Cu	19.04	13.67	40.94	26.50	4.28	0.25
AK0.5Cu	19.04	13.67	40.94	26.50	4.28	0.5

2.2. Material characterizations

Sofosbuvir Differential thermal analysis (DTA, Shimadzu DTG-60H-Japan) for glass powder (size < 0.35 mm) was employed to show the exothermic and endothermic effects and to reveal the transformation and crystallization temperatures of glass powder at a rate of heating (10 ˚C/min).The crystallization phases of the produced samples were determined by X-ray diffraction analysis (XRD, X-ray diffractometer model BRUKER Axs, D8 ADVANCE, Germany). The detector was irradiation at 45kV and 40 mA at an angular range of 5–70° with a step size of 0.02° over 2s conditions and under standard pressure and temperature.

The morphology of the sintered glasses and their elemental microanalysis were investigated with scanning electron microscopy coupled with energy-dispersive x-ray microanalysis, (SEM/EDX SEM Model Quanta Fei,250, Holland).

The functional groups that have been found in the samples were detected by Fourier-transform infrared spectroscopy (FTIR), which has been carried out using a JASCO Asia Portal-FT/IR-4600 FTIR Spectrometer. Additionally, the infrared reflected spectra of the prepared sample have been examined at room temperature (20 °C) with a resolution of 2 cm^{-1}in the spectral region between 400 and 4000 cm^{-1}wavenumbers.

To determine the actual density of the prepared sample, a gas pyrometer was used. A digital balance was employed to determine the specimen's weights (4 digits). By measuring the sample's actual volume, the Gas Pycnometry method establishes the actual density. (Quantachrome Instruments Upyc 1200e V5.03).

The sintered samples at 1000 °C were run through *in-vitro* degradation tests using SBF, according to Kokubo and Takadama) [8] set for pH 7.44 and temperature (37°C). For two and four weeks, the sintered samples were immersed in SBF. Weight loss according to equation (1) and pH changes in the SBF solution were recorded to observe the biodegradation process, and by using an inductively coupled plasma optical emission spectrometer (ICP-OES), the change of calcium, magnesium, and phosphorous ions released from the samples into SBF after several periods was also recorded and analyzed. XRD, (SEM/EDX), and FTIR were used to confirm the creation of the hydroxyapatite layer on the surface of the prepared sample.

$$\text{Weight loss } \% = 100x \frac{W_0(dry) - W_t(dry)}{W_0(dry)} \quad (1)$$

Where W_0 and W_t are mass at the immersion time of (0) and (t).

The agar diffusion method was employed to assess the antimicrobial activity of the prepared samples. Gram-positive (Staphylococcus aureus) and gram-negative (Escherichia coli, Klebsiella pneumoniae, and Pseudomonas aeruginosa) bacteria were used as tested microorganisms [33]. For this, a Luria-Bertani (LB) agar medium plate was injected with a 100 µL bacteria suspension (1×10^6 CFU/mL) By immersing 0.3 g quantities of the materials in medium supplemented with time and incubating at 37 °C for 24 hours, scaffold extracts were created. Then, this LB medium was filled with sterilized 10-mm filter paper discs. As a control, filter paper discs were submerged in sanitized, de-ionized water. These filter paper discs were then layered on top of the agar medium that had been injected with microorganisms, and the dish was then grown for 24 hours at 37 °C. Last but not least, the inhibitory zone was identified using digital camera photos. For each test, we used three equal specimens. The positive control was an antibiotic, while the negative control was water that had been distilled and sterilized. Standard deviation (SD) and student's t-test standard analysis were used in the statistical analysis of all the data for n = 3. The threshold for significance is established at $p < 0.05$.

Employing typical human lung fibroblasts (Wi-38), the cytotoxicity of glass-ceramic powder was assessed in vitro. Before the MTT assay, the cytotoxicity was assessed using the 3-[4,5-dimethylthiazol-yl]-2,5-

diphenyltetrazoliumbromide (MTT) test [34]. Glass-ceramic powder in a range of quantities (31.25–1000 µg/mL) was added to the cell medium for 24 hours. Then, for a further four hours at 37 ºC with 5% CO2, 15 µL of MTT (5 mg/ml) in phosphate-buffered saline (PBS) was added to each well. In order to calculate the number of viable cells and their viability %, the medium was then changed to 1000 µL DMSO, and the absorbance of each well was measured at 570 nm using an ELISA microplate reader (Biochrom ASYS, United Kingdom). The percentage of cell viability is calculated as:

Cell Viability (%) = (average ODt/average ODc) x100

Where: ODt is the average optical density of wells treated with glass ceramic; ODc is the average optical density of the untreated cells (control).

Utilizing the Instant and Prism software suite, all data were presented as means with standard deviations (SD) for n = 3 and analyzed using the classic Student's t-test and two-way ANOVA, with Tukey's test for post hoc pairwise comparisons (GraphPad Software, Inc., San Diego, CA, USA). At $p < 0.05$, significance is determined.

3. Results and Discussion

3.1. Characterization of the glass samples

The DTA curves of the current glass powder (AK0 and AK0.5Cu) was shown in Fig.1. It is clear from the DTA curves that the addition of 0.5 Cu2O caused little change in the softening Ts °C shifted from 600 °C (AK0) to 612 °C (AK0.5Cu), while the exothermic Tc °C changed slightly from 830 (AK0) to 832 °C (AK0.5Cu) also there was little change in the peak shape from clear sharp in AK0 glasses to broad form in AK0.5Cu glass. These findings suggested that the presence of Cu2O did not significantly raise the temperature at which glass crystallizes.

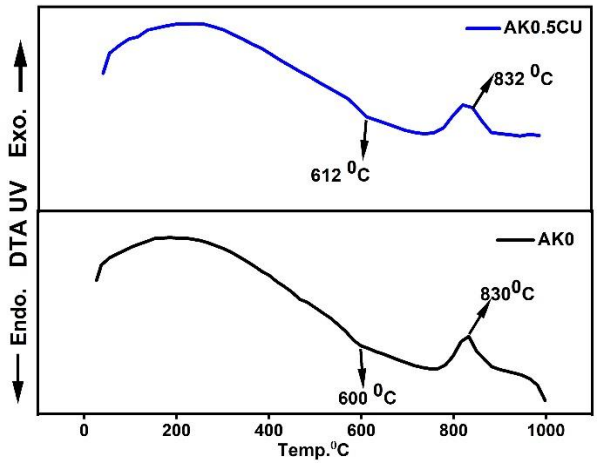

Fig. 1 DTA curves of the (AK0) and AK0.5Cu glasses.

Figure 2 Shows the X-ray diffraction patterns of the glass sintered at 1000 °C /2h. There was a very little amorphous phase in the parent sample and the lines of crystallization were clearer and the glassy phase was limited especially in Cu-containing samples. In addition to the amorphous phase, cuspidine (Ca2Si2F2O7, ICCD#96-901-4741), akermanite (Ca2MgSi2O7, ICCD#96-900-649), and diopside (CaMgSi2O6, ICCD#96-100-0008) were developed in all sintered sample at 1000 ˚C/2h.

Different microstructures can be seen in the SEM images of the glass ceramic discs AK0, AK0.25Cu, and AK0.5Cu sintered at 1000 C/ 2h (Fig. 3). The AK0 sample exhibits particles from the nanoscale to the micron size, wormy-like particles and irregular particles with distinct edges that are either connected or disconnected ridges in the microstructure. Clear clusters irregularly shaped containing interlocked euhedral crystals and some of which have octahedral marking shapes in the scanning electron microscopy of AK0.25Cu.

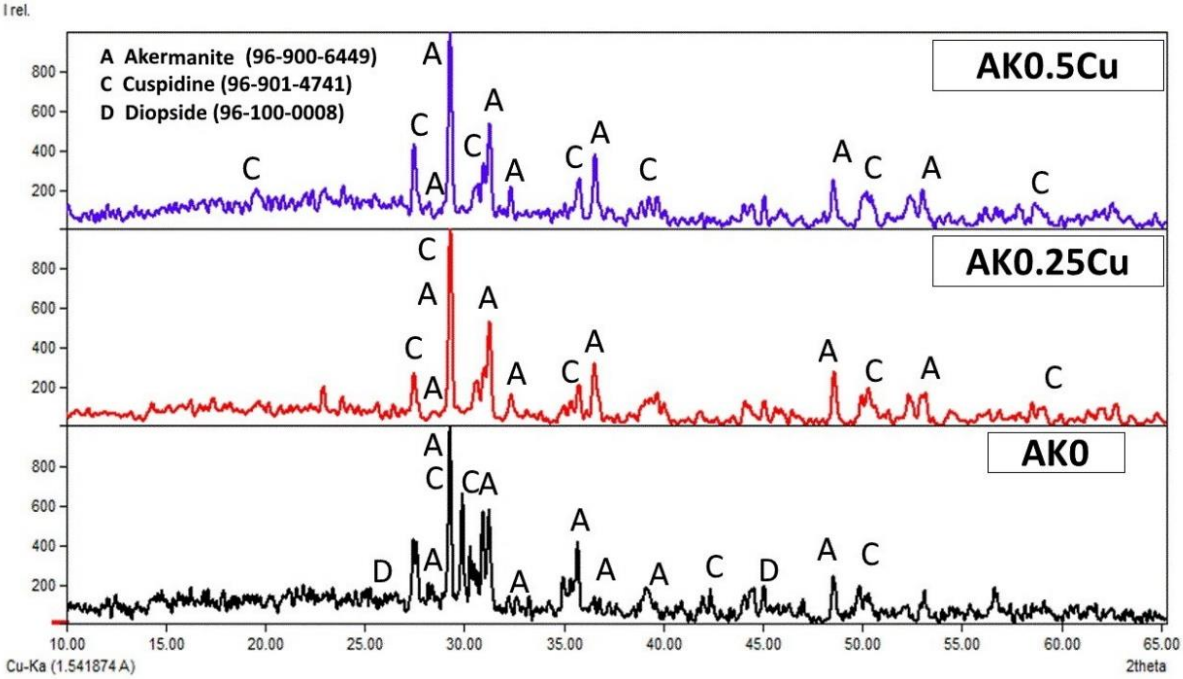

Fig. 2 X-ray diffraction patterns of the glasses sintered at 1000 ˚C/2h

On the other hand, some few euhedral crystals can be spotted in between interconnected clusters of short, interlocking radiated particles in rock surface shape in the scanning electron microscopy of AK0.5Cu. Additionally, EDX analysis was performed on samples AK0, AK0.25Cu, and AK0.5Cu (Fig. 3). All samples displayed the primary peaks of akermanite, which are calcium, magnesium, and silica. Additionally, AK0.25Cu and AK0.5Cu showed that copper peaks were present.

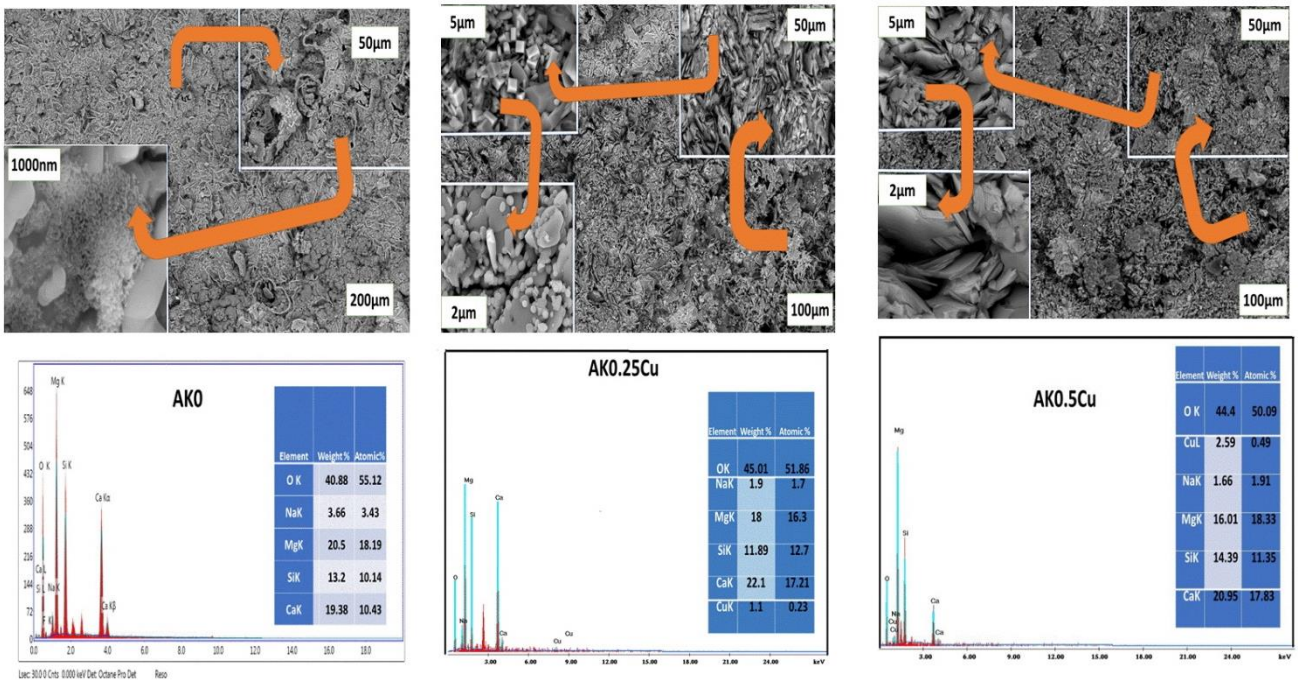

Fig. 3 SEM micrograph and EDX microanalysis of the glass ceramic sintered at 1000°C/2h.

FTIR spectrum of the prepared glass-ceramic samples is illustrated in figure 4. The O-Ca-O bending modes are seen at 418–429 cm^{-1} [26], as well as other bending O-Mg-O at 469–476 cm^{-1}. The presence of the Ca=O group is indicated by the band at 579 cm^{-1}, and the O-Si-O peak, which was observed at 625–650 cm^{-1}, is attributable to the usual vibration modes of Si–O in the SiO_4^{-4} group. The Si-O stretching phases are demonstrated by additional bands at 895 cm^{-1} and 996 cm^{-1} [35]. Additionally, a large moisture absorption band was seen between 3434 and 3447 cm^{-1}. On the other hand, no functional groups were changed by the introduction of copper into the akermanite structure. Finally, Cu-O bond-specific vibrations are difficult to identify since they emerge at wavenumbers lower than 400 cm^{-1} [36].

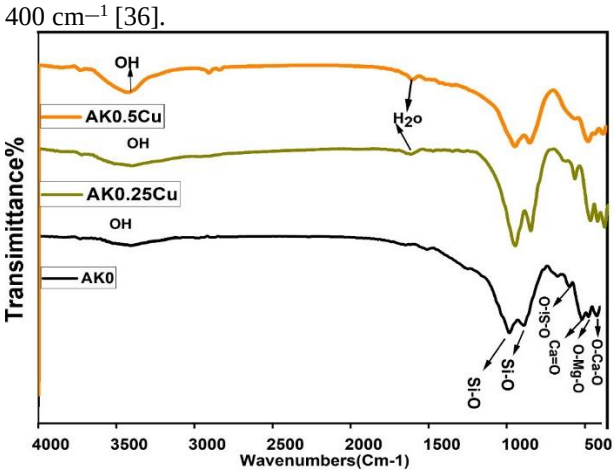

Fig. 4 FTIR spectrum for AK0, AK0.25Cu, and AK0.5Cu samples before immersion in SBF.

3.2. In vitro bioactivity and biocompatibility

By soaking sintered glasses in SBF for 14 and 28 days, the bioactivity and biocompatibility of sintered glasses were examined. XRD, SEM/EDX, and FTIR were used to evaluate the generated samples' surfaces. Studies of density and degradation were also conducted.

3.2.1. X-ray diffraction analysis

The hydroxyapatite was developed in parent glass-ceramic samples and increased in the samples containing Cu_2O. It also showed that after 2 weeks of incubation in SBF, there was some overlapping between phases of akermanite and cuspidine with hydroxyapatite (ICDD:96-210-4756, Ca10.132 (PO4)5.958 (OH) 3.258), but after 4 weeks the phases of akermanite and cuspidine decreased and phases of hydroxyapatite become clearer, especially in Ak0.5Cu samples which emphasis the coverage of sample surface by formed hydroxyapatite.

3.2.2. SEM/EDX analysis

Figures 6 and 7 show SEM images of the surfaces of the prepared samples after immersing in SBF for 14 and 28 days, respectively. Figure 7 also displays the results of the EDX analysis for the samples following their 4-week soaking in SBF. After two weeks of immersion, hydroxyapatite can precipitate on the surfaces of all samples, however, some random surface areas weren't completely coated. The tiny crystals that are distributed amongst several octahedral marking crystals in the SEM micrograph of the AK0 samples indicated that not all of the surfaces have yet been coated by apatite (Fig. 6). The surface of all samples, on the other hand, was nearly completely coated by a coating of spherical

particles after 4 weeks in SBF that indicates the formation of hydroxyapatite (fig.7) [35].

The sample surface's EDX microanalysis after 4 weeks of immersion in SBF revealed the development of a phosphate-containing layer [Fig. 7]. After 4 weeks of immersion, the ratios of Ca/P were 2.91 (AK0), 1.91 (AK0.25Cu), and 1.79. (AK0.5Cu). These results revealed that the parent glass's incorporation of copper raises the phosphate ratio on the sample's surface, which corresponds to the development of the hydroxyapatite layer [Fig.7]. The sample's surface, which is immersed in SBF, begins to create silanol groups (Si-OH) by the action of Si exchange with H+ from the SBF solution. This group serves as a nucleation site for the later creation of the calcium phosphate layer (hydroxyapatite) [37].

3.2.3. FTIR of the samples after soaking in SBF

The FTIR spectra of the AK, AK0.25Cu, and AK0.5Cu glass ceramic specimens after being soaked in SBF for 2 and 4 weeks are shown in Figure 8. In all samples, the soaking in SBF leads to the appearance of new bands matching with the vibration of $(PO_4)^{3-}$. These new bands either cause a diminishing of or the overlapping with the main bands of the tested glass ceramics.

They revealed the presence of rather broad $(PO_4)^{3-}$ bands from 986 to 1100 cm^{-1}. In addition, there are sharp, tiny peaks of bending vibrations of $(PO_4)^{3-}$groups in the calcium phosphate crystal phases from 474 to 529 and 600 to 619 cm^{-1}. Both O-Ca-O and O-Mg-O bands have disappeared completely in samples due to the hydrolysis of calcium and magnesium during the initial stages of the bioactivity test [38], and their places have been occupied by bending vibrations of $(PO_4)^{3-}$ groups in calcium, and phosphate crystal phases.

Also, carbonate bands existed between 1450 -1532 cm^{-1} for all samples in addition to the vibration of the OH group [39,40].

The stretching vibration of the hydrated OH absorbance band was observed (corresponding to 3385 - 3447 cm^{-1}), showing the existence of OH-ions in the apatite layer. The bending vibration of absorbed H_2O was detected at 1658 - 1667 cm^{-1} for all samples at all times of soaking in SBF and abroad. This spectrum has many similarities with the hydroxyapatite crystalline structure [41,42] [Fig. 8]. The figure clears that by increasing the soaking time in SBF the main characteristic bands of hydroxyapatite become dominant with the disappearance of the bands related to the glass-ceramics. Also, the incorporation of Cu_2O in the samples enhances the formation of hydroxyapatite. Previous research has shown that the development of an appetite layer that matches bone on the surface of biomaterials improved in vitro bone regeneration and is one of the key bioactivity evaluation criteria [26].

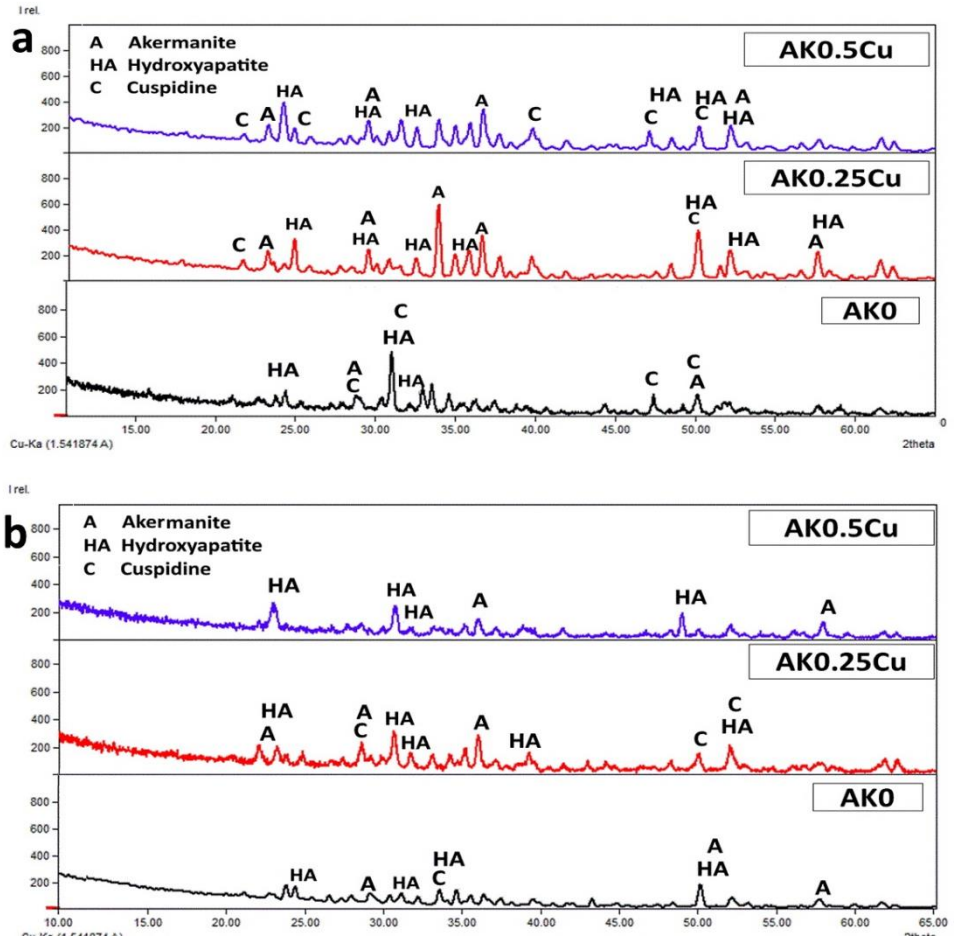

Fig.5 X-ray diffraction patterns of the sintered glass–ceramic surface after soaking in SBF for two (a) and four weeks (b).

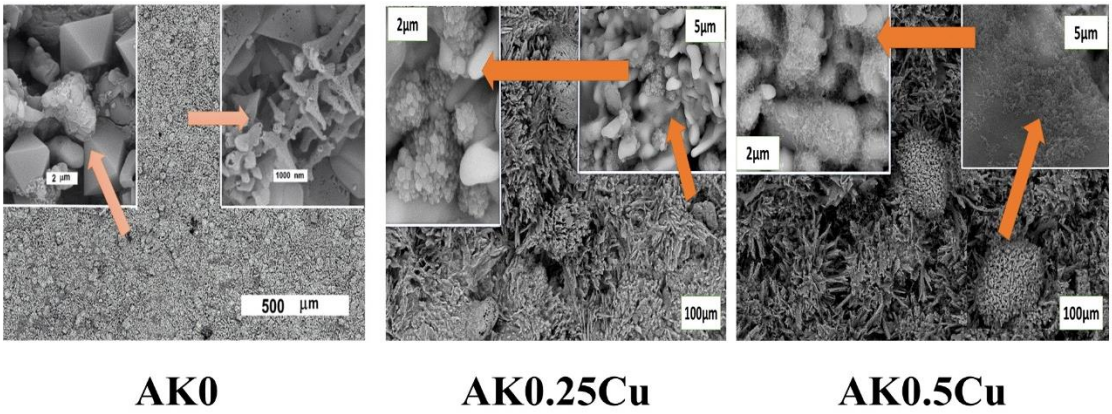

Fig. 6 SEM micrographs of the glass–ceramic AK0, AK0.25Cu, AK0.5Cu soaked in SBF for 2 weeks.

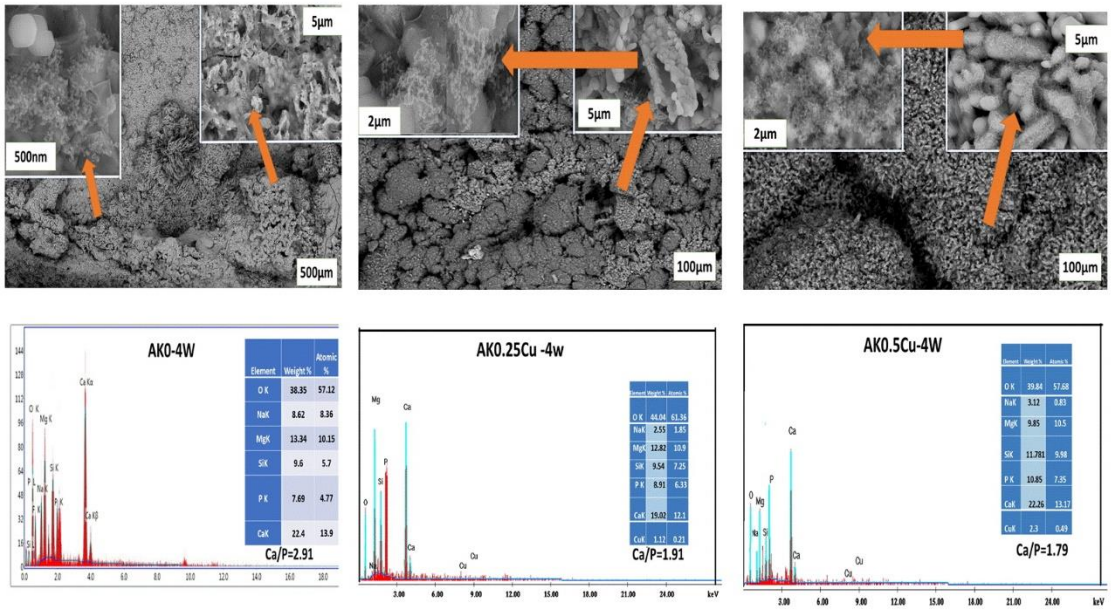

Fig. 7 SEM micrographs of the glass–ceramic AK0, AK0.25Cu, AK0.5Cu soaked in SBF for 4 weeks.

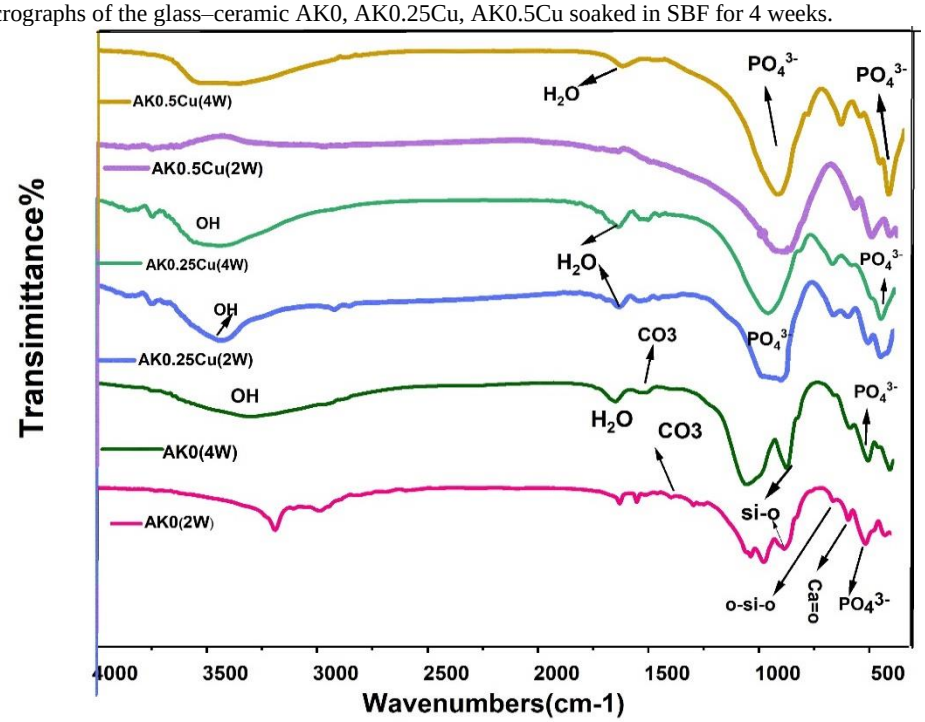

Fig. 8 FTIR spectrum for AK, AK0.25Cu, and AK0.5Cu glasses sintered at 1000 ˚C/2h after soaking in SBF for 2 and 4 weeks.

3.3. Degradation studies

The weight loss percentage, pH changes, calcium, magnesium, and phosphorous ion concentration of the obtained samples following soaking in SBF solution at various periods were all studied.

According to the average weight loss observed for the AK0, AK0.25Cu, and AK0.5Cu samples as a function of the SBF incubation durations (Fig. 9a), all samples had only very minimally regulated biodegradation, it was found that Akermanite bioceramic ($Ca_2MgSi_2O_7$) containing Ca, Mg, and Si have regulated mass loss (up to 3.9%), and as a result, they had beneficial mechanical properties [12,43]. All samples exhibited the same behavior during the whole degradation process, but samples containing copper exhibited weight loss rates that were higher than those of akermanite alone. Lastly, the weight loss detected for the AK0, AK0.25Cu, and AK0.5Cu samples was around 3.590±05, 3.70±044, and 3.90±03, respectively. Additionally, the pH values of all the samples exhibited the same pattern during the immersion time [Fig. 9b]. On the first day of immersion, the pH values of all samples increased from 7.4 to about 7.78, and they then proceeded to increase to 8.001±0.013, 8.09±0.02, and 8.12±0.018 for AK0, AK0.25Cu, and AK0.5Cu, respectively. So, the pH readings, therefore, coincided with the percentage of weight reduction (%). The variations signal in pH marked the beginning of ionic exchanges between the samples and the solution and apatite deposition [44].

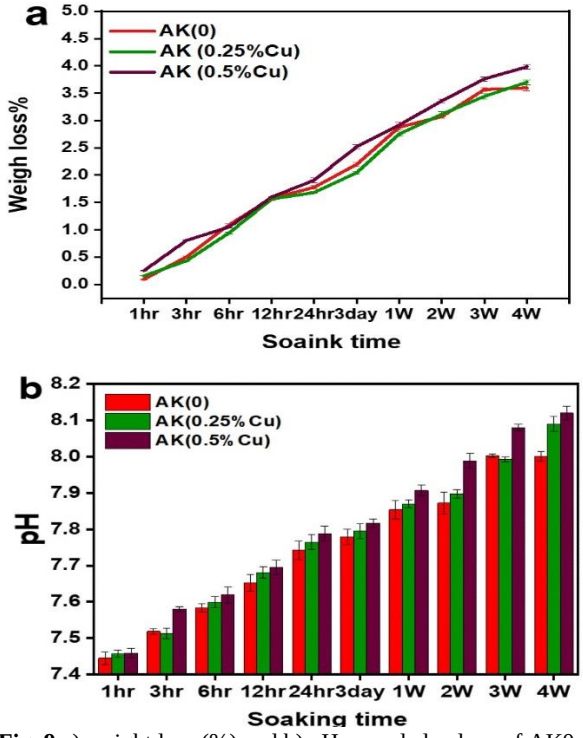

Fig. 9 a) weight loss (%) and b) pH recorded values of AK0, AK0.25Cu, and AK0.5Cu samples in SBF at different soaking times.

As can be seen in Fig. 10, the released calcium, magnesium, and phosphorous ions were evaluated as evidence of the formation of hydroxyapatite.

At different intervals of time, the mean calcium ions concentrations delivered into the SBF solution from the samples were seen in Fig. 10a. It is clear that during the first seven days in all samples, the concentration of Ca2+ ions increased gradually to (18.9 ±0.19), (17.89±0.16) and (18.56±0.23) for AK0, AK0.25Cu, and AK0.5Cu respectively and then decreased slowly. After 28 days of immersion, the calcium ions concentration decreased to 16.61±0.2, 15.4694±0.31, and 16.2998±0.29 for AK0, AK0.25Cu, and AK0.5Cu respectively. The increase in ions released during the period of the first 7 days in all samples was caused by the exchange of calcium ions with H+ or H3O+ions in the solution 37. The deposition of Ca+2 ions onto the surface of the bioactive materials as a result of the attraction of the negative charge of Si-OH groups may be responsible for the subsequent drop in calcium ion concentration in samples [45]. As a result, the degree of the apatite layer may grow. Therefore, it may be claimed that the creation of HA is facilitated by the dissolution of the Ca+2 ions from
the sintered body [36].

Figures 10b and 10c show that the variation in SBF magnesium and phosphorus ion concentration over time was in the opposite direction in several samples. It is clear that the concentration of magnesium ions quickly rose during the first 7 days. After that, gradually, a stable release of magnesium from all the samples was found for up to 28 days Figure 10b, indicating that appetite had covered the surface. This was similar to earlier papers [46]. On the other side, it shows a rapid decrease in the concentration of phosphorous ions Figure 10c, which increases with time. This might be a result of the phosphorus being used in the precipitation of HA layers on sample surfaces. Since P ions were required for the synthesis of HA, it was clearly observed that the drop in P ions in samples with AK0.5Cu was greater than that in samples with AK0 and AK0.25Cu after 21 and 28 days of incubation, respectively. The pH, degradation, and ions produced in SBF are similar to the results shown following immersion in SBF in FTIR and SEM imaging.

3.4. Density measurements

Gas pyrometer measurements of the real densities of the prepared samples are shown in table 2. Before being submerged in SBF, the AK0 had a density of 2.5118 gm/cm^3. This obtained value of the true density is similar to a great extent to that explained by Tavangarian [47]. The addition of Cu_2O at varied amounts (0.25% and 0.5%), resulted in a small difference in the samples' real densities (2.515, and $2.52g/cm^3$). While the values of the prepared samples' real densities varied just a little (2.55, 2.56, and 2.593 g/cm3) after 28 days of incubation in SBF. It was easily noticed that the highest percentage of real density change following incubation in SBF is in the 0.5% Cu_2O containing a sample. Such increase after incubation is attributed to the precipitation of hydroxyapatite onto the surface of samples.

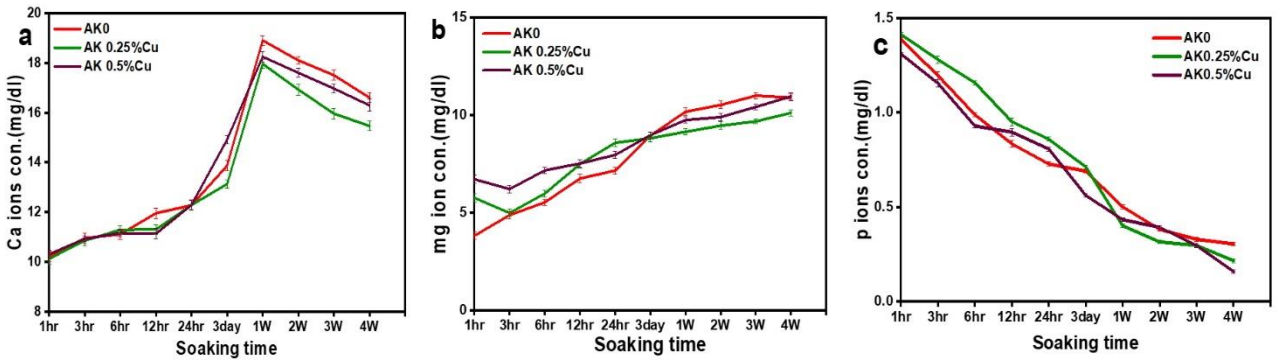

Fig. 10 Ions released in SBF of a) Ca, b) Mg, and c) P from AK0, AK0.25Cu, and AK0.5Cu samples at a different soaking time.

Table 2 real density of samples before and after soaking in SBF and its percent change.

Sample	AK0	AK0.25Cu	AK0.5Cu
Real density before soaking in SBF (g/cm^3)	2.511	2.515	2.52
Real density after soaking in SBF for 28 days (g/cm^3)	2.55	2.56	2.593
Percentage of real density change by the time of soaking	1.553%	1.78%	2.89%

Percentage of real density = real density after soaking – real density before soaking / real density before soaking ×100

3.5. Antibacterial effect of prepared samples

In this work, the antimicrobial efficacy of sintered AK0, AK0.25Cu, and AK0.5Cu samples was examined. Table (3) and figure 11 demonstrate that all prepared samples have an antibacterial effect against the tested gram-negative (*Escherichia coli, Pseudomonas aeruginosa, and Klebsiella pneumonia*) and gram-positive (*Staphylococcus aureus*) bacteria. This effect is indicated by the diameter of the inhibition zone. It is also obvious that the incorporation of Cu_2O enhances the effect of prepared glass ceramic against all tested germs.

The release of alkaline ions such as calcium, which raises the medium's pH and osmolarity and causes cell depression and death of cells, is what gives sintered materials their antibacterial properties [48]. Also, the covering of both gram-positive and gram-negative bacteria by molecules with a negative charge provides them with a higher affinity to positive ions that are released from sintered samples, which leads to cellular losses [49].

Additionally, in this work, copper is a component of glass-ceramic, and studies have proven that copper has great antibacterial properties. Reactive oxygen species can be produced by copper (ROS)that interacts with proteins and lipids, which leads to DNA fragmentation and cell death [50,51,52]. The results showed that the prepared samples have antibacterial properties, and copper doping enhances these antibacterial properties. So, each of these prepared samples can be used to further investigations for usage in medical applications.

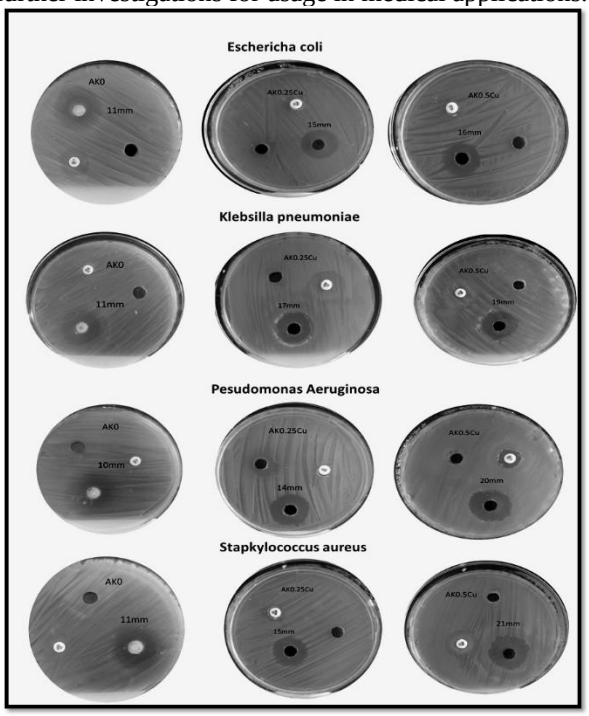

Fig. 11 The inhibition zone diameter (mm) of AK0, AK0.25Cu, and AK0.5Cu against *Escherichia coli*, *Klebsiella pneumoniae*, *Pseudomonas aeruginosa*, and *Staphylococcus aureus*.

Table 3. Samples inhibition zone diameter (in millimeters)

Sample No.	Diameter of inhibition zone (mm)			
	Gram-negative bacteria			Gram-positive bacteria
	Escherichia coli	*Klebsiella pneumoniae*	*Pseudomonas aeruginosa*	*Staphylococcus aureus*
AK0	11±0.31	11±0.36	10±0.21	11±0.73
AK0.25Cu	15±0.52	17±0.71	14±0.68	15±0.59
AK0.5Cu	16±0.28	19±0.35	20±0.51	21±0.47

3.6. Cytotoxicity effect of prepared samples

To assess the biocompatibility of the prepared sintered samples and the effect of Cu_2O doping, their cytotoxicity against human lung fibroblast (Wi-38) cells was evaluated by MTT assay. The results of cytotoxicity of samples AK0, and AK0.5Cu are shown in figure 12 (a, and b). According to the findings (Fig.12, a), the two tested samples have no toxic effect up to 125 µg/ml (micro gram) and the cell viability was close to 100% for all samples at doses of 31.25, 62.5, and 125µg/ml. However, at a concentration of 250ug/ml, the incorporation of Cu_2O (Ak0.5Cu) decreased the cell viability to 85.804%, whereas for Ak0, the viability was nearly 100%. The results also declare that the doping by Cu_2O diminished the IC50 from 617.19±4.23 µg/ml in AK0 to 524.41µg/ml in AK0.5Cu. The viability of cells was decreased in a concentration-dependent way.

Moreover, light microscopy was used to assess the cellular proliferation upon the treatment of human lung fibroblast (Wi-38) cells with AK0, and AK0.5Cu (fig.12, b). it is obvious from the images that up to 125µg/ml, the two tested samples are biocompatible and can be incorporated into the human body without any cytotoxicity on Wi-38 cells. Additionally, due to the toxic effect of copper [53], the cell viability was decreased dramatically when using AK0.5Cu samples at concentrations from 260µg/ml and up.

Since both samples are biocompatible, they can be employed as materials for tissue regeneration. From our result, we can show that copper ions are cytotoxic above a specific concentration and that various cells respond differently to copper ions' cytotoxicity [51,53].

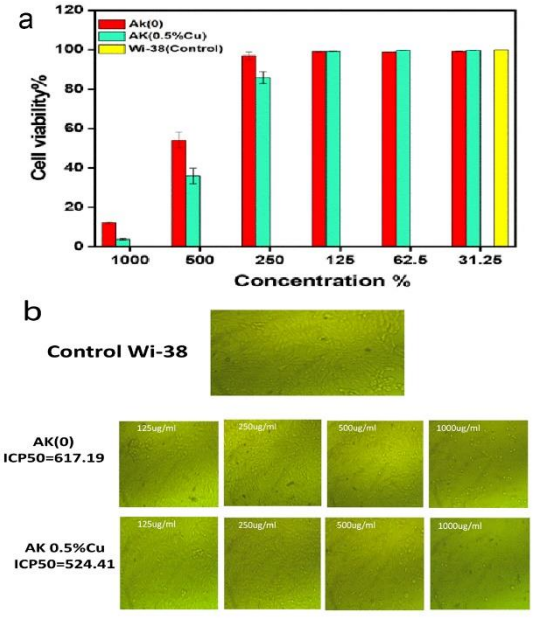

Fig. 12 (a) Cell viability % and (b) Morphological features obtained by optical microscope after 24 hours for WI-38 cells treated with sample concentrations (125, 250, 500, and 1000 µg /ml).

4. Conclusion

Akermanite glass-ceramics ($Ca_2MgSi_2O_7$) ± Cu_2O were prepared by melting quenching method and their thermal behavior was assessed using DTA, XRD, and SEM/EDX techniques. Cuspidine, akermanite, and diopside were developed in the sintered glass samples. the microstructures display grains that are submicron and nanoscale in size. The sintered glasses exhibited a good bioactivity, antibacterial activity, and cytotoxicity at 1000 °C. However, these glass ceramics' antibacterial and bioactive properties were enhanced by the copper present in them. When compared to normal cells, their cytocompatibility test revealed reasonable and similar cell viability.

Acknowledgments

The Authors thank all the help from The Service Laboratories especially the Central Laboratories in the National Research Center.

Declaration of competing interest

The authors declare that there are no conflicts of interest regarding the publication of this paper.

Funding

The present research did not receive any specific grant from funding agencies in the public, commercial, or not-for-profit sectors.

References

1. A. V .Volkov, A.A.Muraev, I.I. Zharkova, V.V.Voinova, E.A.Akoulina, V.A.Zhuikov,,& A.P. Bonartsev, Poly (3-hydroxybutyrate)/hydroxyapatite/ alginate scaffolds seeded with mesenchymal stem cells enhance the regeneration of critical-sized bone defect. Materials Science and Engineering.C. (114) (2020) 110991. https://doi.org/10.1016/j.msec.2020.110991.
2. L. L. Hench and J. K. West, Biological Applications of Bioactive Glasses,Life Chemistry Reports. 13, (1996) 187-241.
3. C.Wu, J.Chang, & Y.Xiao, Mesoporous bioactive glasses as drug delivery and bone tissue regeneration platforms. Therapeutic Delivery. 2(9) (2011)1189-1198. https://doi.org/10.4155/tde.11.84.
4. J.Chevalier, & L.Gremillard, Ceramics for medical applications: A picture for the next 20 years. JournaloftheEuropeanCeramicSociety.29(7)(2009)1245-1255. https://doi.org/10.1016/j.jeurceramsoc.2008.08.025.
5. L. L. Hench, The future of bioactive ceramics. Journal of Materials Science: Materials in Medicine. 26(2) (2015)1-4. https://doi.org/10.1007/s10856-015-5425-3.
6. K. Lin, C. Lin, & Y. Zeng, High mechanical strength bioactive wollastonite bioceramics sintered from nanofibers. RSC advances. 6(17) (2016) 13867-13872. DOI: 10.1039/C5RA26916D
7. F.Tancret, J.M.Bouler, J.Chamousset, & L.M. Minois, Modelling the mechanical properties of microporous and macroporous biphasic calcium phosphate bioceramics. Journal of the European Ceramic Society. 26(16) (2006)3647-3656. https://doi.org/10.101612.015.
8. T. Kokubo, & H.Takadama, How useful is SBF in predicting in vivo bone bioactivity. J. Biomaterials. 27(15) (2006)2907-2915. https://doi.org/10.1016/j.biomaterials.2006.01.017

9. S. Kapoor, A.Goel, A.Tilocca, V.Dhuna, G.Bhatia, K.Dhuna, &J.M. Ferreira, Role of glass structure in defining the chemical dissolution behavior, bioactivity and antioxidant properties of zinc and strontium co-doped alkali-free phosphosilicate glasses. Acta Biomaterialia.10(7)(2014) 3264-3278. https://doi.org/10.1016.03.033.
10. M.Myat-Htun, A.F.M.Noor, M.Kawashita, & Y.M.B. Ismail, Tailoring mechanical and in vitro biological properties of calcium–silicate based bioceramic through iron doping in developing future material. journal of the mechanical behavior of biomedical materials. 128(2022)105122. https://doi.org/10.1016/j.jmbbm.2022.105122.
11. T. Kokubo, H.M. kim, & M. Kawashita, Novel bioactive materials with different mechanical properties. J. Biomaterials. 24(2003) 2161. https://doi.org/10.1016/S0142-9612(03)00044-9.
12. N.Gomez, & C.E. Schmidt, Nerve growth factor-immobilized polypyrrole: Bioactive electrically conducting polymer for enhanced neurite extension. Journal of biomedical materials research. Part A81(1)(2007) 135-149. https://doi.org/10.1002/jbm.a.31047
13. H.B.J. McEntire, B.S. Bal, M.N. Rahaman, J. Chevalier, & G. Pezzotti, Ceramics and ceramic coatings in orthopaedics. Journal of the European Ceramic Society. 35(16) (2015) 4327-4369. https://doi.org/10.1016/j.jeurceramsoc.2015.07.034
14. H. Mohammadi, Y.M.B. Ismail, K.A.B. Shariff, & A.F.M. Noor, Synthesis and characterization of akermanite by mechanical milling and subsequent heat treatment. In Journal of Physics.1082 (1) (2018)012021. DOI 10.1088/1742-6596/1082/1/012021
15. R. Choudhary, S.Koppala, &S. Swamiappan, Bioactivity studies of calcium magnesium silicate prepared from eggshell waste by sol–gel combustion synthesis. Journal of Asian Ceramic Societies. 3(2)(2015)173-177. https://doi.org/10.1016/j.jascer.2015.01.002
16. P. Feng, C. Gao, C. Shuai, & S. Peng, Toughening and strengthening mechanisms of porous akermanite scaffolds reinforced with nano-titania. RSC advances. 5(5) (2015) 3498-3507. DOI: 10.1039/C4RA12095G.
17. C. Wu, J. Chang, W. Zhai, S. Ni, & J. Wang, Porous akermanite scaffolds for bone tissue engineering: preparation, characterization, and in vitro studies. Journal of Biomedical Materials. 78(1) (2006) 47-55.https://doi.org/10.1002/jbm.b.30456
18. F. Ghorbani, A. Zamanian, A. Behnamghader, & M.D. Joupari, Microwave-induced rapid formation of biomimetic hydroxyapatite coating on gelatin-siloxane hybrid microspheres in 10X-SBF solution. e-Polymers.18(3) (2018)247-255. https://doi.org/10.1515/epoly-2017-0196
19. S. Aday, & M. Gümüşderelioğlu, Bone-like apatite-coated chitosan scaffolds: Characterization and osteoblastic activity. Polymer composites, 31(8) (2010)1418-1426. https://doi.org/10.1002/pc.20927.
20. B. Mavis, T.T.Demirtaş, M. Gümüşderelioğlu, G. Gündüz, & Ü. Çolak,. Synthesis, characterization and osteoblastic activity of polycaprolactone nanofibers coated with biomimetic calcium phosphate. Acta biomaterialia.5(8)(2009)3098-3111. https://doi.org/10.1016/j.actbio.2009.04.037
21. Y. Huang, X.Jin, X. Zhang, H.Sun, J. Tu, T. Tang, & K. Dai, In vitro and in vivo evaluation of akermanite bioceramics for bone regeneration. Biomaterials. 30(28)(2009) 5041-5048. https://doi.org/10.1016/j.biomaterials.2009.05.077.
22. T. Kokubo, Bioactive glass ceramics: properties and applications. Biomaterials, 12(2)(1991) 155-163. https://doi.org/10.1016/0142-9612(91)90194-F.
23. C. Wu, & J. Chang, Degradation, bioactivity, and cytocompatibility of diopside, akermanite, and bredigite ceramics. Journal of Biomedical Materials Research Part B: Applied Biomaterials,83(1) (2007)153-160. https://doi.org/10.1002/jbm.b.30779
24. S. Deepthi, J. Venkatesan, S.K. Kim, J.D. Bumgardner, & R. Jayakumar,An overview of chitin or chitosan/nano ceramic composite scaffolds for bone tissue engineering. International journal of biological macromolecules, 93(2016)1338-1353. https://doi.org/10.1016/j.ijbiomac.2016.03.041
25. X. Zhang, & Y. Zhang, Tissue engineering applications of three-dimensional bioprinting. Cell biochemistry and biophysics, 72(3)(2015)777-782. https://doi.org/10.1007/s12013-015-0531-x.
26. L. Chen, D. Zhai, C.Wu, & J. Chang, Poly (d, l-lactic)-reinforced akermanite bioceramic scaffolds: Preparation and characterization. Ceramics International. 40 (8) (2014)12765-12775. https://doi.org/10.1016/j.ceramint.2014.04.130
27. E. Karamian, M. Abdellahi, & H. Gheisari, Fluorine-substituted HA reinforced with zircon as a novel nano-biocomposite ceramic: Preparation and characterization. International Journal of Materials Research.106 (12) (2015) 1285-1290. https://doi.org/10.3139/146.111307.
28. H.E. Götz, M. Müller, A. Emmel, U. Holzwarth, R.G. Erben, & R. Stangl, Effect of surface finish on the osseointegration of laser-treated titanium alloy implants. Biomaterials, 25(18)(2004)4057-4064. https://doi.org/10.1016/j.biomaterials.2003.11.002
29. H. Y. Juang, & M. H. Hon, Effect of calcination on sintering of hydroxyapatite. Biomaterials.17(21)(1996)2059-2064. https://doi.org/10.1016/0142-9612(96)88882-X.
30. J. Zhang, J. Nie, Q. Zhang, Y. Li, Z. Wang, &Q. Hu, Preparation and characterization of bionic bone structure chitosan/hydroxyapatite scaffold for bone tissue engineering. Journal of Biomaterials Science, Polymer Edition.25(1)(2014)61-74. https://doi.org/10.1080/09205063.2013.836950
31. I. Kashif, A.A. Soliman, E.M. Sakr, & A.Ratep, Effect of different conventional melt quenching technique on purity of lithium niobate (LiNbO3) nano crystal phase formed in lithium borate glass. Results in Physics. 2(2012)207-211. https://doi.org/10.1016/j.rinp.2012.10.003.
32. S. C. A. Pina, R. L. Reis, & J. M. Oliveira, Ceramic biomaterials for tissue engineering. 3(2018). DOI: 10.1016/B978-0-08-102203-0.00004-4.
33. M. Prabhu, S. Ruby Priscilla, K. Kavitha, P. Manivasakan, V. Rajendran, & P. Kulandaivelu, In vitro bioactivity and antimicrobial tuning of bioactive glass nanoparticles added with neem (Azadirachta indica) leaf powder. BioMed research international.10(2014). https://doi.org/10.1155/2014/950691.

34. P. R.Twentyman, & M. A. Luscombe, study of some variables in a tetrazolium dye (MTT) based assay for cell growth and chemosensitivity. British journal of cancer. 56(3)(1987)279-285. https://doi.org/10.1038/bjc.1987.190.
35. *M.H. Myat, M.N. Ahmad-Fauzi, K. Masakazu, & B.I Yanny Marliana, In vitro Bioactivity of Copper-doped Akermanite Ceramic. Malaysian Journal of Microscopy, 15(1) (2019).https://malaysianjournalofmicroscopy.org/ojs/index.php/mjm/article/view/388*
36. V. Giannoulatou, G.S. Theodorou, T. Zorba, E. Kontonasaki, L. Papadopoulou, N. Kantiranis, & K.M. Paraskevopoulos, Magnesium calcium silicate bioactive glass doped with copper ions; synthesis and in-vitro bioactivity characterization. Journal of Non-Crystalline Solids.500(2018)98-109. https://doi.org/10.1016/j.jnoncrysol.2018.06.037.
37. A. E. Omar, H. S. Zayed, & E. Hamzawy, Characterization, bioactivity, and antimicrobial activity of CuO-containing devitrite glass–ceramic. Applied Physics A. 128(1) (2022) 1-12. https://rdcu.be/c7pc6
38. M.G. Cerruti, Characterization of bioactive glasses. Effect of the immersion in solutions that simulate body fluids. IJIRSE) International Journal of Innovative Research in Science & Engineering,(2004).
39. M. Głąb, S. Kudłacik-Kramarczyk, A. Drabczyk, J. Walter, A. Kordyka, M. Godzierz, & A. Sobczak-Kupiec, Hydroxyapatite obtained via the wet precipitation method and PVP/PVA matrix as components of polymer-ceramic composites for biomedicalapplications. Molecules, 26(14)(2021).4268. https://doi.org/10.3390/molecules26144268.
40. I. Mobasherpour, M.S. Heshajin, A. Kazemzadeh, & M. Zakeri, Synthesis of nanocrystalline hydroxyapatite by using precipitation method. Journal of Alloys and Compounds, 430(2)(2007) 330-333. https://doi.org/10.1016/j.jallcom.2006.05.018
41. S. Duman, & B. Bulut, Effect of akermanite powders on mechanical properties and bioactivity of chitosan-based scaffolds produced by 3D-bioprinting. Ceramics International.47(10)(2021)13912-13921. https://doi.org/10.1016/j.ceramint.2021.01.258
42. L. Berzina-Cimdina, & N. Borodajenko, Research of calcium phosphates using Fourier transform infrared spectroscopy. Infrared spectroscopy-materials science, engineeringand technology, 12(7)(2012) 251-263.
43. C. Wu, J. Chang, &Y. Xiao, Mesoporous bioactive glasses for drug delivery and bone tissue regeneration. Therapeutic Delivery, 2(9)(2011) 1. https://doi.org/10.4155/tde.11.84.
44. S. Sadeghzade, R. Emadi, & S. Labbaf, Hardystonite-diopside nanocomposite scaffolds for bone tissue engineering applications. Materials Chemistry and Physics,202(2017)95-103. https://doi.org/10.1016/j.matchemphys.2017.09.018
45. J. R. Jones, E. Gentleman, &J. Polak,Bioactive glass scaffolds for bone regeneration. Elements.3(6) (2007) 393-399. https://doi.org/10.2113/GSELEMENTS.3.6.393.
46. C. Wu, J. Chang, J. Wang, S. Ni, & W. Zhai, Preparation and characteristics of a calcium magnesium silicate (bredigite) bioactive ceramic. Biomaterials. 26 (16)(2005)2925-2931. https://doi.org/10.1016/j.biomaterials.2004.09.019
47. F. Tavangarian, C.A. Zolko, S. Sadeghzade, M.Fayed, & K. Davami, Fabrication, mechanical properties and in-vitro behavior of akermanite bioceramic. Materials. 13(21)(2020)4887. https://doi.org/10.3390/ma13214887
48. M.S. Kairon Mbina, S. Shailajha, R. Sankaranarayanan, & L. Saranya, In vitro bioactivity, mechanical behavior and antibacterial properties of mesoporous SiO2-CaO-Na2O-P2O5 nano bioactive glass ceramics. Journal of the Mechanical Behavior of Biomedical Materials, 100(2019)103379. https://doi.org/10.1016/j.jmbbm.2019.103379.
49. Y. N. Slavin, J. Asnis, U.O. Häfeli, & H. Bach, Metal nanoparticles: understanding the mechanisms behind antibacterial activity. Journal of nanobiotechnology.15 (1) (2017)1-20. https://doi.org/10.1186/s12951-017-0308-z
50. A. Jacobs, G. Renaudin, C. Forestier, J.M Nedelec & S. Descamps, Biological properties of copper-doped biomaterials for orthopedic applications: A review of antibacterial, angiogenic and osteogenic aspects. Acta biomaterialia. 117(2020) 21-39. https://doi.org/10.1016/j.actbio.2020.09.044.
51. S. Pang, D. Wu, F. Kamutzki, J. Kurreck, A. Gurlo, & D.A. Hanaor, High performing additively manufactured bone scaffolds based on copper substituted diopside. Materials & Design. 215(2022) 110480. https://doi.org/10.1016/j.matdes.2022.110480.
52. P. Kaur, K.J. Singh, A.K. Yadav, H. Sood, S. Kaur, R. Kaur, & S. Kaur, Preliminary investigation of the effect of doping of copper oxide in CaO-SiO2-P2O5-MgO bioactive composition for bone repair applications. Materials Science and Engineering.C (83) (2018)177-186. https://doi.org/10.1016/j.msec.2017.09.006.
53. S.Gomes, C.Vichery, S.Descamps, H.Martinez, A. Kaur, A.Jacobs, & G.Renaudin,. Cu-doping of calcium phosphate bioceramics: From mechanism to the control of cytotoxicity. Acta Biomaterialia. 65(2018)462-474. https://doi.org/10.1016/j.actbio.2017.10.028